BIOCHEMISTRY
including biophysical chemistry & molecular biology

Article

pubs.acs.org/biochemistry

Human UDP-α-D-xylose Synthase Forms a Catalytically Important Tetramer That Has Not Been Observed in Crystal Structures

Samuel J. Polizzi,[†] Richard M. Walsh, Jr.,[†] Pierre Le Magueres,[‡] Angela R. Criswell,[‡] and Zachary A. Wood*[,†]

[†]Department of Biochemistry and Molecular Biology, University of Georgia, Athens, Georgia 30602, United States
[‡]Rigaku Americas Corp, The Woodlands, Texas 77381, United States

ABSTRACT: Human UDP-α-D-xylose synthase (hUXS) is a member of the extended short chain dehydrogenase/reductase (SDR) family of enzymes. Previous crystallographic studies have shown that hUXS conserves the same dimeric quaternary structure observed in other SDR enzymes. Here, we present evidence that hUXS also forms a tetramer in solution that is important for activity. Sedimentation velocity studies show that two hUXS dimers undergo a concentration-dependent association to form a tetramer with a K_d of 2.9 μM. The tetrameric complex is also observed in small-angle X-ray scattering (SAXS). The specific activity for the production of the reaction intermediate UDP-α-D-4-keto-xylose displays a hyperbolic dependence on protein concentration that is well modeled by an isotherm using the 2.9 μM K_d of the tetramer. Likewise, the rate of UDP-α-D-xylose production in the presence of increasing concentrations of the small molecule crowder trimethylamine *N*-oxide is consistent with the formation of a higher activity tetramer. We present several possible structural models of the hUXS tetramer based on (i) hUXS crystal packing, (ii) homology modeling, or (iii) *ab initio* simulated annealing of dimers. We analyze the models in terms of packing quality and agreement with SAXS data. The higher activity of the tetramer coupled with the relative instability of the complex suggests that an association−dissociation mechanism may regulate hUXS activity.

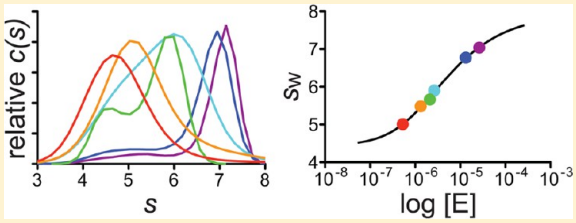

UDP-α-D-xylose (UDP-Xyl) is the essential sugar donor in the biosynthesis of most proteoglycans,[1−3] α-dystroglycan,[4] and Notch receptors.[5] UDP-Xyl is the product of human UDP-xylose synthase (hUXS; E.C. 4.1.1.35), a member of the "extended" subfamily of short chain dehydrogenase/reductase (SDR) enzymes.[6,7] The hUXS mechanism is divided into sequential oxidation and reduction reactions that recycle a bound NAD^+ cofactor (Figure 1A). In the first step, hUXS uses the NAD^+ cofactor to oxidize UDP-α-D-glucuronic acid (UDP-GlcA) to the reaction intermediate UDP-α-D-4-keto-xylose (UDP-4-keto-xylose). Next, it uses the NADH produced in the first step to reduce the intermediate to UDP-Xyl. Because hUXS contains a tightly bound cofactor that is recycled during turnover, there is no need for exogenous NAD^+ in the reaction. Despite this observation, exogenous NAD^+ appears to stimulate hUXS activity.[8,9] We have recently shown that this apparent stimulation is actually due to an abortive catalytic cycle.[9] During turnover, hUXS can release the NADH and UDP-4-keto-xylose intermediates to generate the inactive apoenzyme (Figure 1B).[9] The release of intermediates is slow relative to the production of UDP-Xyl, meaning that only a small fraction of the apoenzyme is produced during each turnover. The apparent stimulatory effect of exogenous NAD^+ is due to the rescue of the resulting apoenzyme. As a result of the bifurcated mechanism, hUXS will slowly produce both UDP-Xyl and the intermediates NADH and UDP-4-keto-xylose in the presence of saturating NAD^+.

The crystal structures of hUXS reveal two domains conserved in all extended SDR enzymes:[8−10] a catalytic domain containing a Rossmann fold for binding the NAD^+ cofactor and a smaller domain for binding the nucleotide-sugar substrate (Figure 1C). hUXS is unique among extended SDR enzymes in that it also contains an N-terminal membrane-spanning domain that anchors the enzyme to the luminal side of the ER/Golgi.[11,12] The crystal structures show that two chains of hUXS associate to form a dimeric structure that is conserved in almost all members of the SDR family. While most extended SDR enzymes function as dimers, some have also been shown to form tetramers arranged as a "dimer of dimers".[13−15]

Here we describe the solution structure of hUXS. We show for the first time that two hUXS dimers weakly associate to form a higher activity tetramer that has not been observed in any of the available crystal structures. Using small-angle X-ray scattering (SAXS), we evaluate five possible tetrameric structures. The higher activity of the relatively unstable tetrameric complex suggests that an association−dissociation mechanism may regulate the enzyme.

Received: March 7, 2013
Revised: May 3, 2013
Published: May 8, 2013

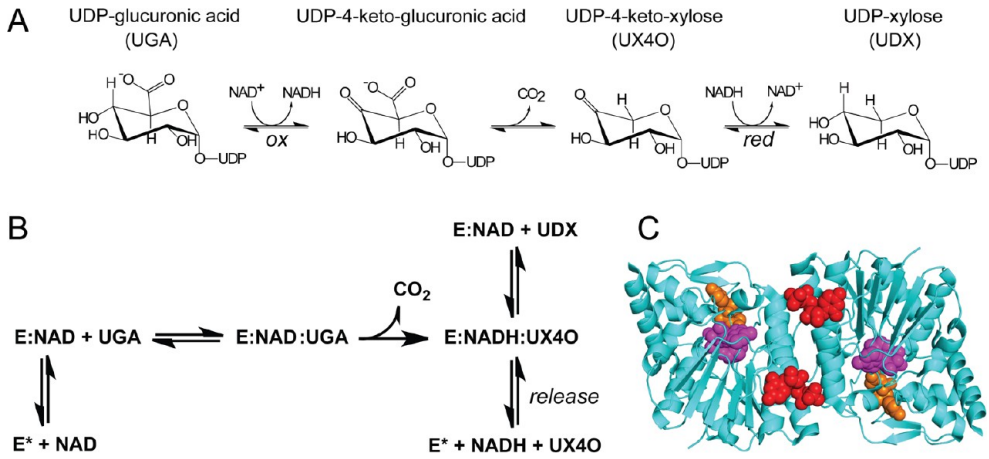

Figure 1. hUXS mechanism. (A) hUXS catalyzes the NAD^+-dependent oxidation and decarboxylation of UDP-glucuronic acid (UGA) to produce the stable intermediates UDP-4-keto-xylose (UX4O) and NADH. Next, the UX4O intermediate is reduced to produce UDP-xylose (UDX) and regenerate the NAD^+ cofactor. (B) hUXS oxidizes UGA to form the intermediate ternary complex (E:NADH:UX4O). The hUXS mechanism is bifurcated in that there are two possible paths for the E:NADH:UX4O complex.[9] In the preferred path, the UX4O is reduced to produce UDX and regenerate the NAD^+ cofactor. In the second path the E:NADH:UX4O complex slowly releases the intermediates. The resulting apoenzyme (E*) can be rescued by exogenous NAD^+. (C) The hUXS:UDP structure (PDB entry 2B69) depicting NAD^+ (magenta spheres) and UDP bound in the active site (orange spheres) or dimer interface (red spheres).

MATERIALS AND METHODS

Sedimentation Velocity Analytical Ultracentrifugation. hUXS lacking the N-terminal membrane spanning domain was expressed and purified as previously reported.[16] Purified protein was concentrated to 790 μM (ε_{280} = 37485 M^{-1} cm^{-1}) in a storage buffer containing 0.2 M NaCl and 25 mM Tris pH 8.0. For sedimentation velocity experiments, hUXS was diluted to 53 μM and dialyzed into phosphate-buffered saline pH 7.5 using a Microdialyzer System (Pierce), then diluted to the final concentration for analysis. 400 μL of diluted sample or reference PBS buffer was loaded into 12 mm double-sector Epon centerpieces equipped with quartz windows and equilibrated at 20 °C in an An60 Ti rotor for 1 h. Sedimentation velocity data were collected in an Optima XLA analytical ultracentrifuge using a rotor speed of 50 000 rpm at 20 °C. Data were recorded at a wavelength of 230 nm for protein concentrations of 0.5, 1, and 2 μM, or 280 nm for 3, 13, and 26 μM samples using a radial step size of 0.003 cm. The partial specific volume (V-bar) of 0.7353 was calculated from the amino acid sequence of truncated hUXS. The buffer viscosity of 1.019 Poise and density of 1.00564 g/mL were calculated using the program SEDNTERP[17] (www.bbri.org/RASMB). Sedimentation velocity data were analyzed using the programs SEDFIT and SEDPHAT (www.analyticalultracentrifugation.com). Continuous sedimentation coefficient distribution $c(s)$ analyses were restrained by maximum entropy regularization at P = 0.68 confidence interval.[18] The baseline, meniscus, frictional coefficient, systematic time-invariant and radial-invariant noise were fit. The weight-averaged sedimentation coefficient (s_w) was determined by integrating each $c(s)$ distribution over the range of interacting species, then converted to standard conditions (water at 20 °C) and plotted versus hUXS loading concentration. Global analysis was used to fit the $c(s)$ distribution data to the appropriate self-association model.[19] Theoretical sedimentation coefficient (s) values were calculated from hUXS atomic coordinates under standard conditions using HYDROPRO[20] (www.bbri.org/RASMB).

Small-Angle X-ray Scattering (SAXS) Structural Analyses. hUXS was exchanged into SAXS buffer (200 mM NaCl, 50 mM phosphate pH 7.5, 5% glycerol) and diluted to the working concentration. Sample and buffer data were collected at 4 °C in 5 and 30 min exposures using Cu K_α radiation from a Rigaku FR-E+ Superbright rotating anode X-ray generator and a Rigaku BioSAXS-1000. The BioSAXS-1000 uses confocal multilayer optics, Kratky collimation, a Dectris Pilatus 100K detector, and a 500 mm sample to detector distance. Experiments covered a q range of 0.009−0.69 $Å^{-1}$. The absence of radiation damage was verified by inspecting 5-min exposures (data not shown). Using the Rigaku SAXSLab software, sample and buffer images were converted from pixel space to q-space to produce 1D plots of "I vs q". Data were corrected for buffer scattering with PRIMUS.[21] The experimental radius of gyration (R_g) was computed (for sR_g < 1.3) using AUTORG.[22] The monomer dry volume was estimated from the amino acid sequence using NucProt (www.molmovdb.org).[23] The oligomer Porod volume was calculated with DATPOROD.[22] The oligomer molecular weight was determined using SAXMoW (www.if.sc.usp.br/~saxs).[24] Oligomer models were refined by simulated annealing using SASREF.[25] Calculated scattering profiles and R_g from atomic coordinates were determined with CRYSOL.[26] Buried surface area, Δ^iG and the associated P-value, and interface residues were calculated using the PISA server (http://www.ebi.ac.uk/pdbe/prot_int/pistart.html).[27] Figures were generated with PyMOL (http://www.pymol.org).

Enzyme Assays. Standard enzyme assays, unless otherwise stated, contained 50 mM Tris pH 8.0, 10 mM DTT (Research Products International), 1 mM EDTA, and 2 mM UDP-glucuronic acid (UDP-GlcA; Sigma-Aldrich). All reactions were initiated by addition of substrate following a 5 min preincubation at 25 °C. The steady state production and release of reaction intermediates was assayed in the standard reactions containing 2.5 mM NAD^+ (Sigma-Aldrich) and 1.3−79 μM hUXS. Samples were placed in a 1 cm quartz cuvette, and changes in absorbance at 340 nm (for NADH formation) were recorded using a Agilent 8453 UV−vis spectrophotometer

dx.doi.org/10.1021/bi400294e | Biochemistry 2013, 52, 3888−3898

equipped with a Peltier temperature controller set at 25 °C. Absorbance was converted to concentration using the molar extinction coefficient of NADH (ε_{340} = 6220 M^{-1} cm^{-1}). Initial velocities for UDP-Xyl and NADH production were corrected for enzyme concentration to obtain specific activity.

For assaying the effect of molecular crowding on the rate of UDP-Xyl production, reactions contained 0.3 μM hUXS and increasing concentrations (0.25−1.5 M) of trimethylamine *N*-oxide (TMAO; Sigma-Aldrich). To quantitate UDP-Xyl produced, samples were taken at regular time intervals and plunged into liquid nitrogen. Samples were then vortexed with 1:1 v/v chloroform to thaw, centrifuged to obtain the aqueous phase, boiled for 5 min, and re-extracted with 1:1 v/v chloroform. The aqueous layer was loaded to a capillary electrophoresis system (Agilent Technologies) in an uncoated, fused-silica capillary (560 mm × 50 μm) with an extended light path (Agilent Technologies) at 18 °C, separated via capillary zone electrophoresis in 20 mM borate pH 9.3 run buffer for 20 min at 22 kV capillary voltage, and monitored at 260 nm wavelength light. Chromatograms were analyzed with the Agilent CE ChemStation, and UDP-Xyl was identified by comigration with known standards. The UDP-Xyl peak area was manually integrated and converted to molar concentration using a standard curve of known UDP-sugar concentrations.

Modeling the Dependence of UDP-4-Keto-xylose Production on Protein Concentration. The specific activity for UDP-4-keto-xylose production displays a hyperbolic dependence on protein concentration, suggesting the formation of a more active tetramer (see Results). On the basis of the predicted dimer K_d of 67 nM (see Results), we treated the amount of monomer in the protein concentration used in this analysis (1.3−79 μM hUXS) as negligible. Thus, we begin our derivation assuming an equilibrium between two low activity dimers (E_D) and a higher activity tetramer (E_T):

$$2E_D \overset{K_a}{\leftrightarrow} E_T$$

The tetramer concentration can be expressed as

$$[E_T] = K_a[E_D]^2 \quad (1)$$

The total concentration of enzyme, $[E_{total}]$ is

$$[E_{total}] = 2[E_D] + 4[E_T] \quad (2)$$

which can be expressed in terms of the dimer concentration:

$$[E_{total}] = 2[E_D] + 4K_a[E_D]^2 \quad (3)$$

or

$$0 = 4(K_a)[E_D]^2 + 2[E_D] - [E_{total}] \quad (4)$$

Using the general solution for a quadratic equation, we solve for $[E_D]$ in terms of total enzyme concentration:

$$[E_D] = \frac{-2 + \sqrt{4 + 16K_a[E_{total}]}}{8K_a} \quad (5)$$

The specific activity (SA) of hUXS is the sum of the specific activities of the tetramer (SA_T) and dimer (SA_D) multiplied by their molar fraction:

$$SA = \frac{4[E_T]}{[E_{total}]}SA_T + \frac{2[E_D]}{[E_{total}]}SA_D \quad (6)$$

Expressing the SA in terms of the concentration of dimer (eq 1):

$$SA = \frac{4K_a[E_D]^2}{[E_{total}]}SA_T + \frac{2[E_D]}{[E_{total}]}SA_D \quad (7)$$

By substituting eq 5 for $[E_D]$ in the above expression, we can solve for total specific activity in terms of total enzyme concentration. Specific activity data at different enzyme concentrations were fit using the program PRISM (GraphPad Software, Inc.).

RESULTS

Human UXS Forms a Tetramer in Solution. We analyzed the solution structure of hUXS lacking the N-terminal membrane-spanning domain (hUXS; residues 85−420) using sedimentation velocity analytical ultracentrifugation (Figure 2A). The sedimentation of 0.5 μM hUXS reveals a single broad peak centered at 4.6 S, close to the calculated value of the dimer (5.0 S) based on the hUXS crystal structures (Figure 1A, Table

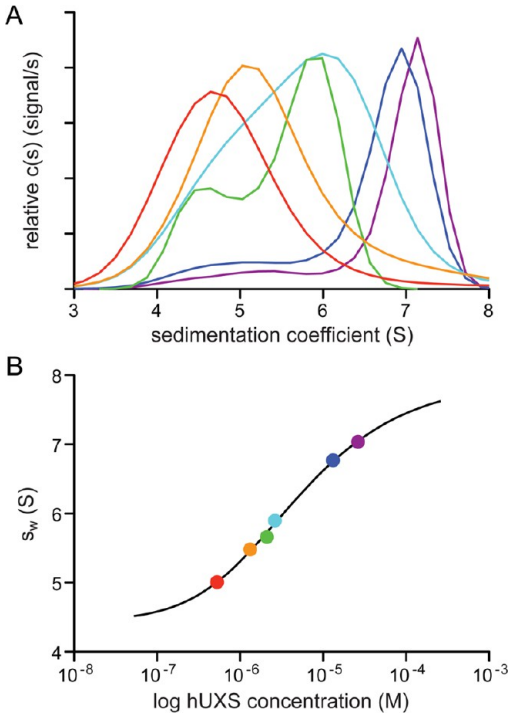

Figure 2. Sedimentation velocity analysis shows hUXS forms a concentration-dependent tetramer in solution. (A) Overlay of *c*(*s*) distributions calculated from various concentrations of hUXS: 0.5 μM (red), 1 μM (orange), 2 μM (green), 3 μM (cyan), 13 μM (blue), and 26 μM (purple). The different *c*(*s*) distributions were scaled to ease comparison. (B) The weight averaged *s*-values (s_w) from each of the *c*(*s*) distributions (colored as above) plotted against protein concentration. Data are globally fit to a monomer−dimer−tetramer association binding isotherm using SEDPHAT.[37]

Table 1. Hydrodynamic Properties of the hUXS Oligomers

oligomer	s_{calc} (S)[a]	$s_{modeled}$ (S)[b]	K_d (μM)[b]
monomer	3.3	3.5	
dimer	5.0	5.1	0.067
tetramer		7.9	2.890

[a]Sedimentation coefficient (*s*) values were calculated with HYDRO-PRO[20] using atomic coordinates from PDB entry 4GLL. [b]*s*-values and K_d from the monomer−dimer-tetramer association modeled in SEDPHAT.[37]

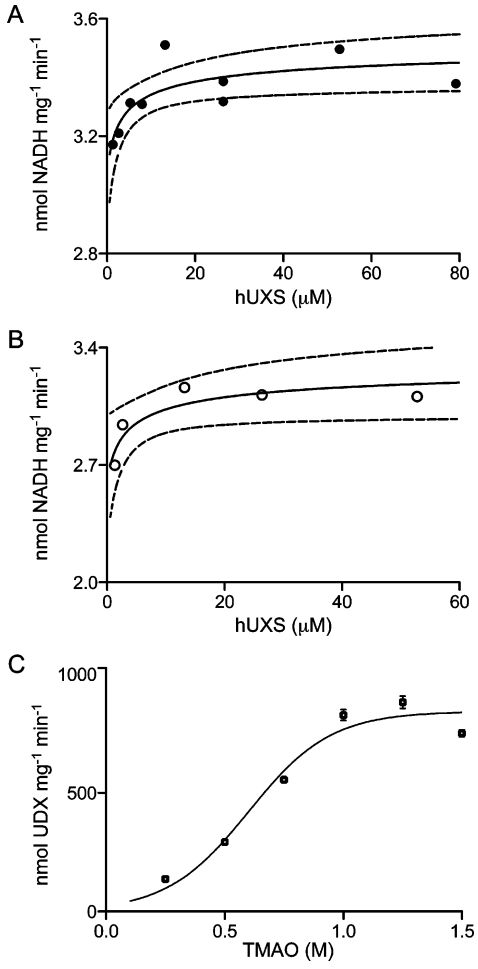

Figure 3. The hUXS tetramer is more active than the dimer. (A) The production and release of NADH is plotted as a function of increasing hUXS concentrations in Tris pH 8.0. Data are fit with eq 7 (see Methods), and the K_d of 2.9 μM derived from the sedimentation velocity analysis. 95% confidence intervals are depicted with dashed lines. (B) Same as in (A) above, but in phosphate pH 7.5 buffer. (C) UDP-Xyl production is shown as a function of crowding in reactions containing 0.26 μM hUXS and increasing concentrations of the molecular crowder trimethylamine *N*-oxide (TMAO). An S-curve is superimposed onto the specific activity data to illustrate the similarity to a binding isotherm. Each data point represents the average of three replicates, and error bars depict standard deviation.

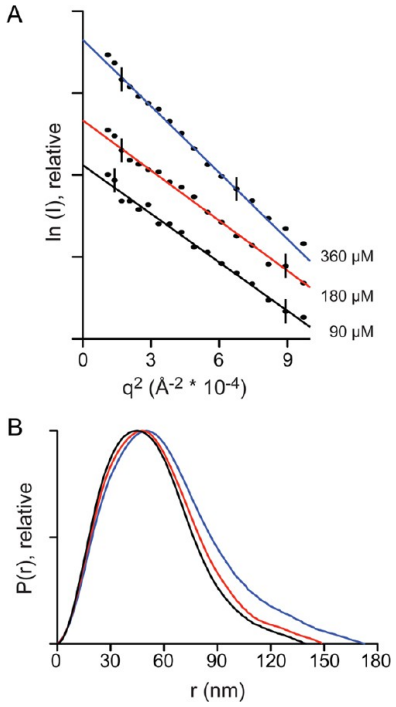

Figure 4. The tetramer is observed in small-angle X-ray scattering (SAXS). (A) Guinier analyses of SAXS data for 360 μM (blue), 180 μM (red) and 90 μM hUXS (black). The linear Guinier region used for calculating the radius of gyration (sR_g < 1.3) is identified by hash marks on the fit line. (B) Pair distance distribution plots for each dilution are scaled for ease of comparison.

1). The width of the peak and tailing at larger *s*-values suggests the presence of a dynamic equilibrium with a larger oligomeric species. We also observe a slight tailing at lower *s*-values indicating a small amount (~20%) of monomer (predicted to sediment at 3.3 S). At higher concentrations of hUXS, the distribution shifts to larger *s*-values, converging to a species around 7 S (Figure 2A). The amount of monomer decreases at higher protein concentrations, suggesting that the monomer is due to the reversible dissociation of the dimer. At the highest concentration tested (26 μM hUXS), the distribution is modeled as a peak at 7 S that is continuous with a slower sedimenting species at 5 S (Figure 2A). The sedimentation velocity data from all protein concentrations was modeled using global analysis. The weight-averaged sedimentation coefficients (s_w) from each $c(s)$ distribution were fit to a monomer−dimer−tetramer association model (Figure 2B). This model predicts a 3.5 S monomer, 5.1 S dimer, and 7.9 S tetramer, consistent with the calculated values (from crystal structures) of 3.3 and 5.0 S for monomer and dimer, respectively (Table 1). The model also predicts dissociation constants of 67 nM and 2.9 μM for the dimer and tetramer, respectively (Table 1).

The hUXS Tetramer Is the Catalytically Important Species. The hUXS mechanism is bifurcated,[9] meaning that after the initial oxidation step, the enzyme can either release NADH and UDP-4-keto-xylose as products, or reduce the reaction intermediates to produce UDP-Xyl (Figure 1B). Because the release of the intermediates is much slower than the reduction step, the production of UDP-Xyl is the preferred path in the mechanism. To determine the contribution of the tetramer to hUXS activity, we measured the rates for both paths under conditions that favor tetramer formation. First, we measured the rate of the production and release of the reaction intermediates NADH and UDP-4-keto-xylose at different protein concentrations using a previously described assay.[9] The specific activity for the production of intermediates displays a hyperbolic dependence on protein concentration in both Tris (pH 8.0) and phosphate (pH 7.5) buffers (Figure 3A,B). The data are well modeled by an equation relating specific activity to protein self-association (eq 7) using the K_a ($1/K_d$) of the hUXS tetramer determined from the sedimentation velocity analysis above. At Tris pH 8.0, the model predicts specific activities of 3.1 ± 0.1 and 3.5 ± 0.1 nmol mg^{-1} min^{-1} for the dimer and tetramer, respectively. Similarly, in phosphate pH 7.5, the model predicts specific activities of 2.6 ± 0.1 and 3.3 ± 0.1 nmol mg^{-1} min^{-1} for the dimer and tetramer, respectively.

Next, we examined the effect of the hUXS tetramer on the production of UDP-Xyl. We are not able to accurately measure the rate of UDP-Xyl production at the high protein

dx.doi.org/10.1021/bi400294e | *Biochemistry* 2013, 52, 3888−3898

Table 2. Data Collection and Scattering-Derived Parameters

Data collection parameters	
instrument	BioSAXS-1000 (Rigaku)
beam geometry	700 μm × 200 μm (at sample position)
	500 μm × 500 μm (at detector)
wavelength (Å)	1.5418
q range (Å^{-1})	0.0105−0.634
exposure time (min)	30
concentration (μM)	90
temperature (K)	277
Structural Parameters[a]	
$I(0)$ (cm^{-1}) [from P(r)]	2.93 ± 0.03
R_g (Å) [from P(r)]	40.84 ± 0.43
$I(0)$ (cm^{-1}) [from Guinier]	3.02 ± 0.03
R_g (Å) [from Guinier]	42.1 ± 0.58
D_{max} (Å)	140
porod volume estimate (Å^3)	262398
dry volume calculated from sequence (Å^3)	47003
Molecular mass determination[a]	
partial specific volume from sequence (cm^3 g^{-1})	0.7353
calculated monomeric M_r from sequence (Da)	37873
Software employed	
primary data reduction	*SAXSLab*
data processing	*PRIMUS*
rigid-body modeling	*SASREF*
computation of model intensities	*CRYSOL*
three-dimensional graphics representation	*PyMOL*

[a]Reported for 90 μM hUXS buffered in 200 mM NaCl, 50 mM Phosphate pH 7.5 and 5% glycerol.

concentrations needed to stabilize the tetramer (K_d = 2.9 μM) due to the high velocity of the reaction. Instead, the hUXS concentration was fixed at 0.3 μM, and the specific activity for UDP-Xyl production was determined in the presence of increasing amounts of the molecular crowder TMAO. High concentrations of TMAO have been shown to stabilize native protein oligomeric complexes and promote association-dependent activities.[28,29] Between 0.25 and 1.0 M TMAO, the rate of UDP-Xyl production increases by more than 6-fold (Figure 3C). The dependence of the hUXS rate on TMAO concentration qualitatively resembles an isotherm and is consistent with the formation of a higher activity tetramer (Figure 2B).

Small-Angle X-ray Scattering Reveals a Tetramer Not Observed in the hUXS Crystal Structures. We investigated the solution structure of hUXS using SAXS. The Guinier plot of the X-ray scattering from 360 μM hUXS shows a small, but systematic deviation from linearity, indicating a degree of aggregation at high protein concentrations (Figure 4A). This aggregation is also evident in the calculated molecular weight from SAXS (227.8 kDa), which is significantly greater than the expected molecular weight of the tetramer (151.6 kDa). Reducing the protein concentration ameliorates the aggregation, resulting in consistently linear Guinier plots (Figure 4A). On the basis of the 2.9 μM dissociation constant calculated from the sedimentation velocity experiments, we choose a protein concentration of 90 μM to minimize aggregation while stabilizing the complex (Table 2). At this concentration, the Guinier analysis predicts an R_g of 42 ± 0.5 Å, similar to the R_g of 40.8 ± 0.4 Å estimated from the $P(r)$ distribution (Figure 4). In addition, the SAXS calculated molecular weight of 169.6 kDa is close to the expected tetramer molecular weight (151.6 kDa). It is notable that the R_g from the scattering data is significantly greater than 30.0 Å calculated from atomic coordinates of the hUXS dimer (Figure 4, Table 2).

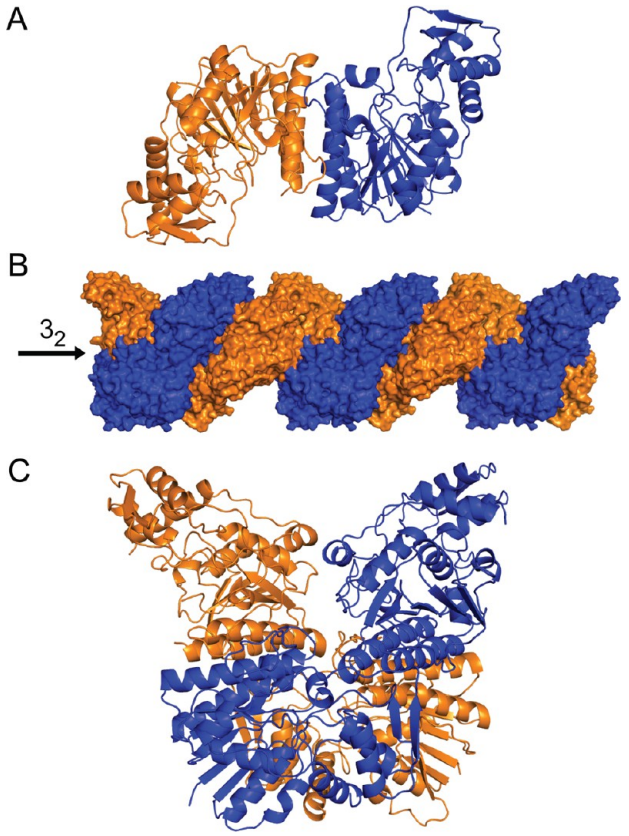

Figure 5. Substrate-free hUXS forms a fiber in the crystal lattice. (A) The asymmetric unit of PDB entry 4GLL contains two monomers (orange and blue) that associate to form the canonical SDR dimer. (B) The dimers make extensive crystal contacts along the crystallographic 3_2 symmetry axis to form a fiber. (C) Two adjacent dimers in the fiber form a putative tetramer.

The crystal structures of substrate-free hUXS (hUXS, PDB entry 4GLL) and hUXS in complex with UDP (hUXS:UDP, PDB entry 2B69) have been previously described (Figures 1C and 5A).[8,9] These structures were solved in different space groups and both reports identified hUXS as a dimer. As expected from the observed R_g, the calculated scattering of the hUXS dimer does not fit the SAXS experimental data (χ = 11.3) (Figure 6A). We examined both hUXS structures for crystal contacts that might identify the authentic hUXS tetramer. In the hUXS:UDP structure, none of the crystal contacts appear to support a higher order assembly (not shown). However, in the substrate-free hUXS structure, we identified an extensive crystal contact that might represent an authentic tetramer interface (Figure 5B,C). This interface buries 4191.8 Å^2 and is formed by dimers packing along the crystallographic 3_2 axis to form a fiber throughout the crystal lattice (Figure 5B). We used PISA to analyze the putative tetramer interface. An authentic interface would be expected to have a favorable solvation free energy gain (Δ^iG), and the likelihood that the surface is interaction-specific (P-value) would be less than <0.5.[27] On the basis of these criteria, the

dx.doi.org/10.1021/bi400294e | *Biochemistry* 2013, 52, 3888−3898

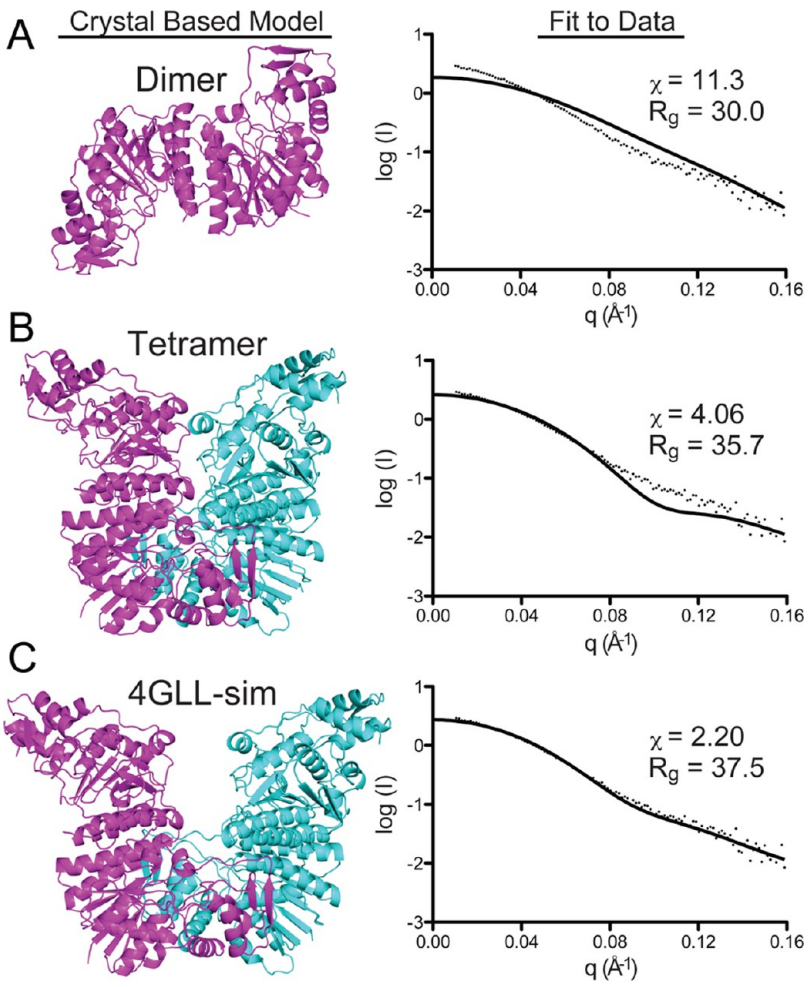

Figure 6. SAXS analysis of crystallographic complexes. The left column (Crystal Based Model) shows dimeric and tetrameric complexes based on the substrate-free hUXS crystal structure (PDB entry 4GLL). The right column (fit to data) depicts theoretical scattering curves (solid lines) generated for each model fit to experimental SAXS data (dots) using CRYSOL.[26] The radius of gyration (R_g) and quality of fit (χ) are shown for each model. (A) The hUXS dimer shows a poor fit to the SAXS data. (B) The crystallographic tetramer has a better fit due to the larger R_g but deviates at larger scattering angles ($q < 0.08$). (C) Restrained simulated annealing was used to refine the crystallographic tetramer against SAXS data to generate 4GLL-sim.

Table 3. hUXS Tetramer Models Refined Using SAXS

modeled tetramers	interface (Å^2)[a]	Δ^iG (kcal mol^{-1})[a]	Δ^iG *P*-value[a]	hydrogen bonds[a]	salt bridges[a]	favorable residues (%)[a]	chi value[b]	R_g (Å)[b]
4GLL[c]	4191.8	−10.7	0.198	10	2	43	4.06	35.7
4GLL-sim	3747.8	8.2	0.882	15	9	54	2.20	37.5
Model 1	3470.6	7.2	0.900	14	4	53	1.97	37.4
Model 2	2141.2	−11.8	0.054	4	0	44	1.90	37.7
Model 3	1238.2	−2.9	0.358	2	0	41	1.66	40.9
Model 4	2086.2	−8.3	0.127	6	4	40	1.62	41.0

[a]Total buried interface, hydrophobic free energy gain (Δ^iG), associated Δ^iG P-value, and favorable residue interactions calculated using PISA.[27] [b]Agreement between experimental SAXS data and theoretical scattering (chi value), or radius of gyration (R_g), calculated using CRYSOL.[26] [c]Tetramer located in the substrate-free hUXS crystal structure (PDB entry 4GLL) (Figure 5C).

substrate-free hUXS structure (Δ^iG = −10.7 kcal mol^{-1}, P = 0.198) contains a possible tetramer (Table 3). Despite the encouraging scores from PISA, the calculated SAXS scattering of the tetramer is a poor match to the experimental data (χ = 4.06) (Figure 6B). We refined the tetramer against the SAXS data using simulated annealing. To maintain the complex, we had to include the following modest distance restraints: (i) the distance between residues 164−169 in monomers B and A′ must be less than 20 Å; (ii) the distance between Asn185 and Glu353′ of monomers A and A′, respectively, must be less than 10 Å, (the same restraint was applied to monomers B and B′). Simulated annealing improved both the χ score (2.20) and the 2-fold symmetry between the AB and A′B′ dimers (Figure 6C). Despite the improved fit to the observed scattering data, the PISA score suggests that the resulting model is unlikely; the interface has an unfavorable free energy (Δ^iG = 8.2 kcal mol^{-1}) and very low likelihood to be interaction specific (P = 0.882) (Table 3). Thus, the available crystal structures of hUXS do not support the tetramer that we observe in our solution studies. The lack of crystallographic evidence for the tetramer is most

dx.doi.org/10.1021/bi400294e | *Biochemistry* 2013, 52, 3888−3898

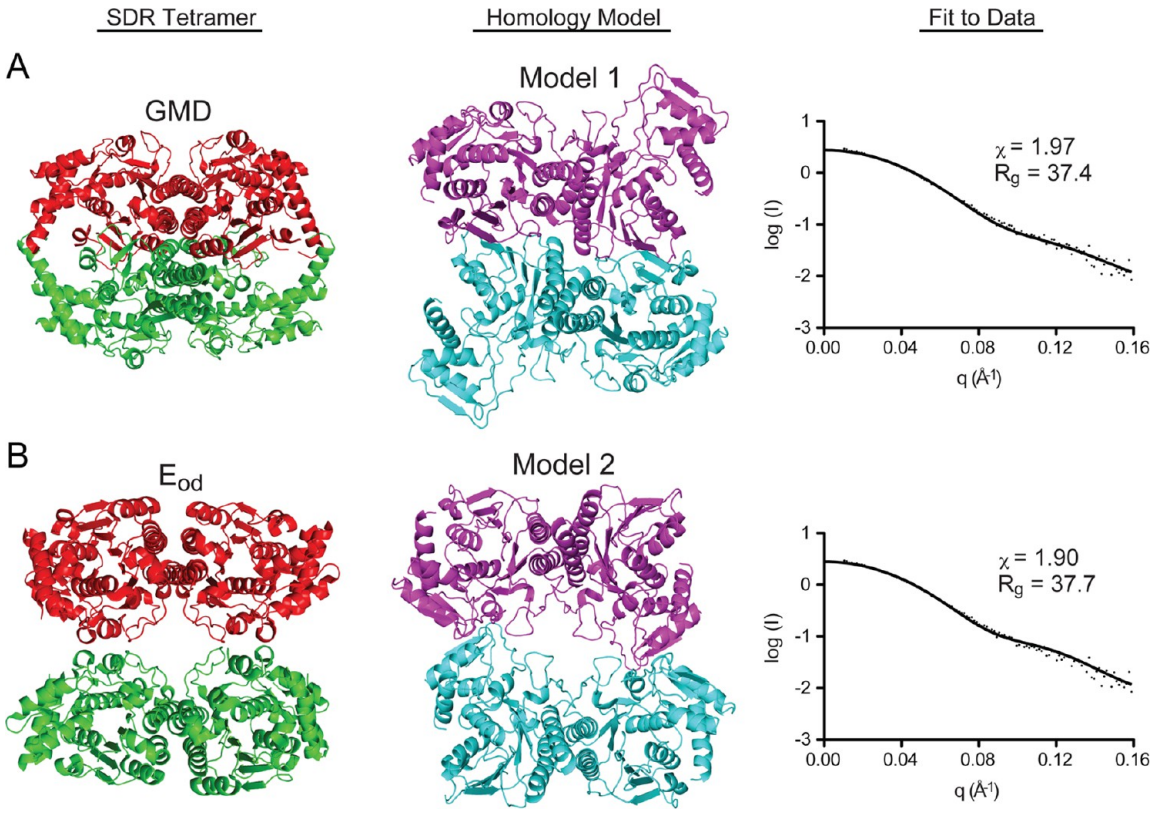

Figure 7. hUXS models based on homologous SDR tetramers. The extended SDR tetramer used as a template for modeling the hUXS tetramer is shown in the left column (SDR tetramer). The modeled hUXS tetramer following restrained simulated annealing refinement against the SAXS data is shown in the middle column (homology model). The agreement between the modeled tetramer and the SAXS data is shown in the far right column (fit to data). The radius of gyration (R_g) and quality of fit (χ) are shown for each model. (A) The *Arabidopsis thaliana* GDP-mannose 4,6-dehydratase (GMD; PDB entry 1N7G) based homology Model 1. (B) The *Yersinia pseudotuberculosis* CDP-glucose 4,6-dehydratase (E_{od}; PDB entry 1RKX) based homology Model 2.

likely due to the relative instability of the complex (see Discussion).

Modeling of Two Distinct Tetrameric Assemblies That Are Consistent with Small-Angle X-ray Scattering. Two types of SDR tetramers have been described (Figure 7A,B): (i) the GMD-type tetramer represented by GDP-mannose 4,6-dehydratase (GMD)[13,30] and CDP-tyvelose 2-epimerase;[15] and (ii) the E_{od}-type tetramer formed by CDP-glucose 4,6-dehydratase (E_{od}).[14,31] Each of these tetramers is formed by the association of two canonical SDR dimers. We generated possible hUXS tetramers based on homology with the GMD and E_{od} enzymes. To generate Model 1, we superimposed two hUXS dimers onto the GMD crystal structure. Initially, Model 1 contained main-chain clashes and poor agreement with the SAXS data (χ = 3.02) (not shown). We refined Model 1 using simulated annealing and the following restraints: (i) P2 symmetry and (ii) the distance between Arg127 in chains A and B′ or A′ and B must be less than 15 Å. The resulting model has no main-chain clashes and displays a better fit to experimental data (χ = 1.97) (Figure 7A). However, the interface in Model 1 has an unfavorable free energy (Δ^iG = 7.2 kcal mol^{-1}) and is unlikely to be interaction-specific (P = 0.900) (Table 3). Because of the poor PISA scores, we do not think Model 1 is likely.

We generated Model 2 by superimposing two hUXS dimers onto the E_{od} tetramer. The initial model also contained main-chain clashes but had a reasonable agreement with the scattering data (χ = 2.03) (not shown). We subjected the model to simulated annealing with the following restraints: (i) P2 symmetry and (ii) the distance between His212 in chains A and B′ or A′ and B must be less than 7 Å. The refined model has no clashes (Figure 7B). The PISA scores for the interface of Model 2 are encouraging, with a favorable free energy (Δ^iG = −11.8 kcal mol^{-1}) and a high probability of being interaction-specific (P = 0.054) (Table 3).

To reduce bias in our modeling of a tetramer, we also performed 10 simulating annealing refinements on two hUXS dimers with only a P2 symmetry restraint (no distance restraints). The solutions from these runs converged to two distinct tetrameric arrangements: Models 3 and 4 (Figure 8). Model 3 represents the most populated group (seven of the simulations) (Figure 8A). The interface in Model 3 is relatively small (1238 Å^2) with relatively weak PISA scores: a favorable Δ^iG (−2.9 kcal mol^{-1}) and likelihood to be interaction-specific (P = 0.358) (Table 3). Thus, Model 3 is not likely to resemble the authentic hUXS complex.

The remaining three simulations converged to a distinct tetramer represented by Model 4 (Figure 8B). Model 4 shows the best agreement with the SAXS data, with a χ = 1.62 (Figure 8B). The Model 4 tetramer is formed by interactions between adjacent nucleotide sugar binding domains (residues 212−215, 291−296, and 325−375). The interface of Model 4 is a reasonable size (2086 Å^2) and has a very favorable Δ^iG (−8.3 kcal mol^{-1}) and a high likelihood to be interaction specific (P = 0.127) (Table 3). Thus, Models 2 and 4 represent our current best approximations of the hUXS tetramer.

dx.doi.org/10.1021/bi400294e | *Biochemistry* 2013, 52, 3888−3898

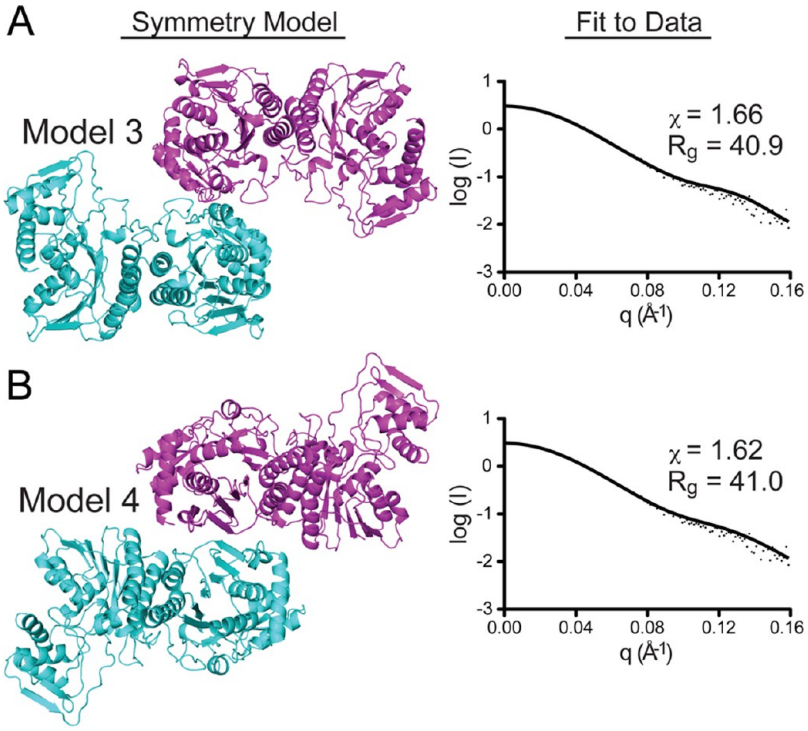

Figure 8. Restrained hUXS tetramer models. The left column (symmetry model) shows the tetramers generated by simulated annealing of two hUXS dimers (PDB entry 4GLL) with only a P2 symmetry restraint. The right column (fit to data) shows the agreement between the model and the SAXS data. The radius of gyration (R_g) and quality of fit (χ) are shown for each model. (A) Seven of the 10 simulations converged to the Model 3 tetramer. (B) The three remaining simulations converged to the Model 4 tetramer.

DISCUSSION

Previous crystallographic studies, including one by our group, have identified the quaternary structure of hUXS as a homodimer.[8,9] Here we have presented strong evidence that hUXS actually forms a catalytically important tetramer in solution. Sedimentation velocity experiments identify a discrete, albeit relatively unstable, hUXS tetramer with a K_d = 2.9 μM (Figure 2). SAXS studies also show that hUXS forms a tetramer in solution based on the observed radius of gyration and calculated mass (Table 2). The relative instability of the hUXS tetramer may be a consequence of the truncated protein construct we used in our analysis. In order to express soluble protein, we removed the N-terminal membrane-spanning domain that anchors the enzyme to the luminal side of the endoplasmic reticulum. Tethering hUXS to a membrane would be expected to increase the stability of the tetramer by decreasing the degrees of freedom. It is also possible that the missing domain directly participates in tetramer formation to further stabilize the complex. Thus, the native, full-length hUXS tetramer will be significantly more stable when attached to the membrane. It is also well-known that macromolecular crowding in a cell greatly enhances weak and transient interactions.[32,33] In fact, we show that a relatively small amount of the molecular crowding agent TMAO can drive 0.26 μM of hUXS to tetramer, despite a weak dissociation constant of 2.9 μM (Figure 3C).

We have presented evidence that the tetramer is important for enzyme activity. hUXS can produce and release the reaction intermediates NADH and UDP-4-keto-xylose during the catalytic cycle (Figure 1).[9] Here we have shown that the rate for the production and release of reaction intermediates displays a hyperbolic dependence on protein concentration that is reminiscent of a binding isotherm (Figure 3A,B). In fact, we can model the change in specific activity using the dissociation constant that we determined from our sedimentation velocity experiments (Figure 3A,B). This model is consistent with two lower activity dimers associating to form a higher activity tetramer (Figure 2B). We have also shown that UDP-Xyl production displays a similar dependency on the concentration of the molecular crowder TMAO (Figure 3C). Crowding agents such as TMAO are known to stabilize oligomeric complexes and promote association-dependent activities.[28,29] While there is not a general equation that will model the dependency of oligomer formation on TMAO concentration, the shape of the specific activity curve is consistent with what one would expect from a protein associating to form a more active tetramer (Figure 3C). We note that the increase in the two activities is not uniform; the rate of UDP-Xyl production increases 6-fold compared to only a 15−20% increase for the release of the reaction intermediates. This may be in part due to the bifurcated reaction mechanism of hUXS (Figure 1). In order to release the reaction intermediates, the structure of hUXS has to undergo a significant localized unfolding to expose the active site.[9] If formation of the tetrameric complex stabilizes the folded conformation of hUXS, it would favor the retention of reaction intermediates and bias the reaction toward the final product UDP-Xyl. It is also possible that some of the discrepancy between the two activities may be due in part to the presence of TMAO in the reaction; TMAO has been shown to increase activity by simply stabilizing the folded, active conformation of a protein.[34,35] Still, the dependence of the rate at which the reaction intermediates are produced is consistent with tetramer formation (Figure 3A,B). We believe that it is likely the increased rate of UDP-Xyl production in the presence of

dx.doi.org/10.1021/bi400294e | Biochemistry 2013, 52, 3888−3898

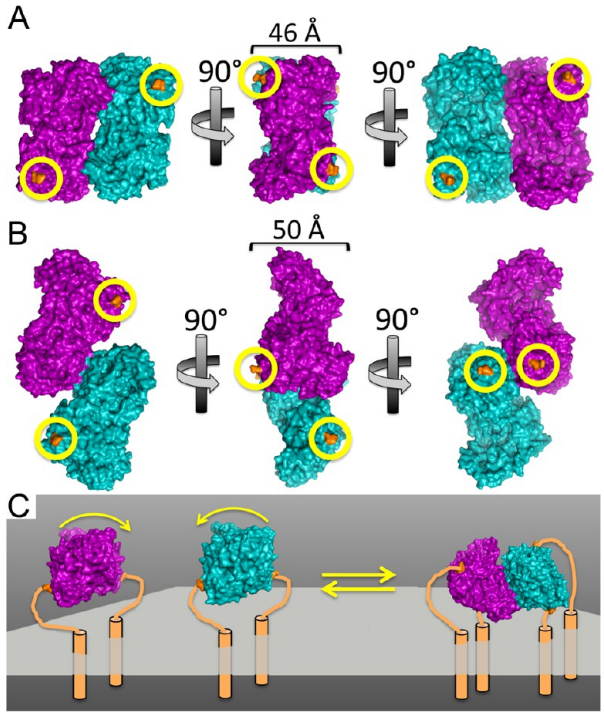

Figure 9. The relationship of the N-termini in the modeled tetramers to the membrane-binding domain. (A) Tetramer Model 2 showing the position of the N-termini (orange circled with yellow) on the two hUXS dimers (purple and teal). The bracket denotes the width of the tetramer. (B) Tetramer Model 4 depicted as in (A). (C) The transmembrane helix (residues 20−38, orange cylinder) and connecting linker (orange loop) are shown connecting to the hUXS dimer. Assuming the 48 residue linker is sufficiently flexible, the rotation of the dimers (curved arrows) can allow formation of the Model 2 tetramer despite the N-termini being separated by the 46 Å width of the tetramer (for reference, the fully extended length of the linker would be 182 Å). The Model 4 tetramer can also form given these constraints (not depicted).

TMAO is likely due to tetramer formation (Figure 3C). It is tempting to speculate that the relative instability of the tetramer may represent a means to regulate enzyme activity. This interpretation suggests a possible means of regulating activity.

None of the current crystal structures of hUXS reveal a tetramer consistent with our solution studies. After an exhaustive search, we identified a single possible tetrameric complex in the crystal structure of substrate-free hUXS (Figure 5). However, this complex does not agree with the SAXS data. Worse yet, the complex is part of a continuous fiber that runs through the crystal lattice, suggesting that conditions that favor tetramer formation would also favor fiber formation (Figure 5B). The absence of the tetramer in the two crystal structures is likely due to the relatively weak tetramer interface (K_d = 2.9 μM). Krissinel and Henrick have suggested that the absence of the authentic quaternary structure in a crystal structure is, in some cases, due to the dissociation of a relatively weak complex during nucleation and crystal growth.[27] Thus, even though the high protein concentrations used in crystallization favor the hUXS tetramer, the relatively small amount of dimer present at equilibrium can feed the growth of a more stable crystal lattice. In the case of substrate-free hUXS, the large, stable crystal contact along the 3_2 symmetry axis is consistent with this interpretation (Figure 5 and Table 3). If the stability of this crystal contact is close to or greater than that of the tetramer interface, it is easy to see how crystallization can compete for tetramer formation, especially under the optimized conditions that favor crystal growth. In the case of the hUXS:UDP structure, there are no comparable, extensive crystal contacts. However, it has been reported that there are two UDP molecules bound in each monomer[8] (Figure 1C), one in the active site and the other in the dimer interface. It may be that the UDP bound at the dimer interface may sterically preclude formation of the tetramer.

We have modeled and analyzed several tetrameric structures of hUXS. Our results suggest that Model 2, based on homology with the E_{od} tetramer (PDB entry 1RKX), is a reasonable complex yielding favorable PISA scores and good agreement with SAXS data (Figure 7B and Table 3). We also employed a less biased approach using simulated annealing restrained by P2 symmetry to produce Model 4 (Figure 8B and Table 3). Models 2 and 4 are structurally distinct (compare Figures 7B and 8B), but both are reasonable complexes based on our criteria. We also considered the relationship of the complex to the membrane. The N-terminal transmembrane helix (residues 20−38) is connected to the soluble fragment by a 48 residue linker.[9,36] Assuming that the linker is flexible, it is possible to connect Models 2 and 4 to the membrane without disrupting the tetrameric complex (Figure 9). To address the ambiguity, we are pursuing new crystallization experiments using proteins with amino acid substitutions designed to disrupt the 3_2 symmetry axis in the substrate-free hUXS crystal structure. Regardless, our present inability to identify the actual structure of the hUXS tetramer should not distract from our key finding. Our results clearly show that hUXS forms a catalytically important tetramer in solution and that the relative instability of the complex suggests a means of regulating activity.

AUTHOR INFORMATION

Corresponding Author

*Phone: 706-583-0304. Fax: 706-542-1783. E-mail: zac@bmb.uga.edu.

Funding

Funding from the University of Georgia Research Alliance and the American Cancer Society Grant (RSG0918401DMC) to Z.A.W. is gratefully acknowledged.

Notes

The authors declare no competing financial interest.

ACKNOWLEDGMENTS

We thank Rigaku for generously donating use of their SAXS facility (The Woodlands, TX). We also thank Huaying Zhao (National Institute of Biomedical Imaging and Bioengineering, NIH) for advice on sedimentation velocity analysis.

ABBREVIATIONS

hUXS, human UDP-xylose synthase; SDR, short-chain dehydrogenase/reductase; SAXS, small-angle X-ray scattering; UDP-Xyl, UDP-α-D-xylose; UDP-GlcA, UDP-α-D-glucuronic acid; UDP-4-keto-xylose, UDP-α-D-4-keto-xylose; s, sedimentation coefficient; $c(s)$, continuous s distribution; s_w, weight averaged s; R_g, radius of gyration; TMAO, trimethylamine N-oxide; GMD, GDP-mannose 4,6-dehydratase; E_{od}, CDP-glucose 4,6-dehydratase

REFERENCES

(1) Bai, X., Zhou, D., Brown, J. R., Crawford, B. E., Hennet, T., and Esko, J. D. (2001) Biosynthesis of the linkage region of glycosaminoglycans: cloning and activity of galactosyltransferase II, the sixth member of the beta 1,3-galactosyltransferase family (beta 3GalT6). *J. Biol. Chem. 276*, 48189−48195.

(2) Silbert, J. E., and Sugumaran, G. (2002) Biosynthesis of chondroitin/dermatan sulfate. *IUBMB Life 54*, 177−186.

(3) Sugahara, K., and Kitagawa, H. (2002) Heparin and heparan sulfate biosynthesis. *IUBMB Life 54*, 163−175.

(4) Inamori, K., Yoshida-Moriguchi, T., Hara, Y., Anderson, M. E., Yu, L., and Campbell, K. P. (2012) Dystroglycan function requires xylosyl- and glucuronyltransferase activities of LARGE. *Science 335*, 93−96.

(5) Takeuchi, H., Fernandez-Valdivia, R. C., Caswell, D. S., Nita-Lazar, A., Rana, N. A., Garner, T. P., Weldeghiorghis, T. K., Macnaughtan, M. A., Jafar-Nejad, H., and Haltiwanger, R. S. (2011) Rumi functions as both a protein O-glucosyltransferase and a protein O-xylosyltransferase. *Proc. Natl. Acad. Sci. U. S. A. 108*, 16600−16605.

(6) Kavanagh, K. L., Jornvall, H., Persson, B., and Oppermann, U. (2008) Medium- and short-chain dehydrogenase/reductase gene and protein families: the SDR superfamily: functional and structural diversity within a family of metabolic and regulatory enzymes. *Cell. Mol. Life Sci. 65*, 3895−3906.

(7) Persson, B., Kallberg, Y., Bray, J. E., Bruford, E., Dellaporta, S. L., Favia, A. D., Duarte, R. G., Jornvall, H., Kavanagh, K. L., Kedishvili, N., Kisiela, M., Maser, E., Mindnich, R., Orchard, S., Penning, T. M., Thornton, J. M., Adamski, J., and Oppermann, U. (2009) The SDR (short-chain dehydrogenase/reductase and related enzymes) nomenclature initiative. *Chemico-Biol. Interact. 178*, 94−98.

(8) Eixelsberger, T., Sykora, S., Egger, S., Brunsteiner, M., Kavanagh, K. L., Oppermann, U., Brecker, L., and Nidetzky, B. (2012) Structure and mechanism of human UDP-xylose synthase: evidence for a promoting role of sugar ring distortion in a three-step catalytic conversion of UDP-glucuronic acid. *J. Biol. Chem. 287*, 31349−31358.

(9) Polizzi, S. J., Walsh, R. M., Jr., Peeples, W. B., Lim, J. M., Wells, L., and Wood, Z. A. (2012) Human UDP-alpha-D-xylose synthase and E. coli ArnA conserve a conformational shunt that controls whether xylose or 4-keto-xylose is produced. *Biochemistry 51*, 8844−8855.

(10) Kallberg, Y., Oppermann, U., Jornvall, H., and Persson, B. (2002) Short-chain dehydrogenases/reductases (SDRs. *Eur. J. Biochem./FEBS 269*, 4409−4417.

(11) Moriarity, J. L., Hurt, K. J., Resnick, A. C., Storm, P. B., Laroy, W., Schnaar, R. L., and Snyder, S. H. (2002) UDP-glucuronate decarboxylase, a key enzyme in proteoglycan synthesis: cloning, characterization, and localization. *J. Biol. Chem. 277*, 16968−16975.

(12) Bakker, H., Oka, T., Ashikov, A., Yadav, A., Berger, M., Rana, N. A., Bai, X., Jigami, Y., Haltiwanger, R. S., Esko, J. D., and Gerardy-Schahn, R. (2009) Functional UDP-xylose transport across the endoplasmic reticulum/Golgi membrane in a Chinese hamster ovary cell mutant defective in UDP-xylose Synthase. *J. Biol. Chem. 284*, 2576−2583.

(13) Mulichak, A. M., Bonin, C. P., Reiter, W. D., and Garavito, R. M. (2002) Structure of the MUR1 GDP-mannose 4,6-dehydratase from Arabidopsis thaliana: implications for ligand binding and specificity. *Biochemistry 41*, 15578−15589.

(14) Vogan, E. M., Bellamacina, C., He, X., Liu, H. W., Ringe, D., and Petsko, G. A. (2004) Crystal structure at 1.8 Å resolution of CDP-D-glucose 4,6-dehydratase from Yersinia pseudotuberculosis. *Biochemistry 43*, 3057−3067.

(15) Koropatkin, N. M., Liu, H. W., and Holden, H. M. (2003) High resolution X-ray structure of tyvelose epimerase from Salmonella typhi. *J. Biol. Chem. 278*, 20874−20881.

(16) Eames, B. F., Singer, A., Smith, G. A., Wood, Z. A., Yan, Y. L., He, X., Polizzi, S. J., Catchen, J. M., Rodriguez-Mari, A., Linbo, T., Raible, D. W., and Postlethwait, J. H. (2010) UDP xylose synthase 1 is required for morphogenesis and histogenesis of the craniofacial skeleton. *Dev. Biol. 341*, 400−415.

(17) Laue, T. M., Shah, B. D., Ridgeway, T. M. & Pelletier, S. L. (1992). Computer-aided interpretation of analytical sedimentation data for proteins. In *Analytical Ultracentrifugation in Biochemistry and Polymer Science* (Harding, S. E., Rowe, A. J., and Horton, J. C., Eds.), pp 90−125, The Royal Society of Chemistry, Cambridge.

(18) Brown, P. H., and Schuck, P. (2006) Macromolecular size-and-shape distributions by sedimentation velocity analytical ultracentrifugation. *Biophys. J. 90*, 4651−4661.

(19) Dam, J., Velikovsky, C. A., Mariuzza, R. A., Urbanke, C., and Schuck, P. (2005) Sedimentation velocity analysis of heterogeneous protein-protein interactions: Lamm equation modeling and sedimentation coefficient distributions c(s). *Biophys. J. 89*, 619−634.

(20) Garcia De La Torre, J., Huertas, M. L., and Carrasco, B. (2000) Calculation of hydrodynamic properties of globular proteins from their atomic-level structure. *Biophys. J. 78*, 719−730.

(21) Konarev, P. V., Volkov, V. V., Sokolova, A. V., Koch, M. H. J., and Svergun, D. I. (2003) PRIMUS: a Windows PC-based system for small-angle scattering data analysis. *J. Appl. Crystallogr. 36*, 1277−1282.

(22) Petoukhov, M. V., Konarev, P. V., Kikhney, A. G., and Svergun, D. I. (2007) ATSAS 2.1 - towards automated and web-supported small-angle scattering data analysis. *J. Appl. Crystallogr. 40*, 223−228.

(23) Voss, N. R., and Gerstein, M. (2005) Calculation of standard atomic volumes for RNA and comparison with proteins: RNA is packed more tightly. *J. Mol. Biol. 346*, 477−492.

(24) Fischer, H., De Oliveira Neto, M., Napolitano, H. B., Polikarpov, I., and Craievich, A. F. (2010) Determination of the molecular weight of proteins in solution from a single small-angle X-ray scattering measurement on a relative scale. *J. Appl. Crystallogr. 43*, 101−109.

(25) Petoukhov, M. V., and Svergun, D. I. (2005) Global rigid body modeling of macromolecular complexes against small-angle scattering data. *Biophys. J. 89*, 1237−1250.

(26) Svergun, D., Barberato, C., and Koch, M. H. J. (1995) CRYSOL - a Program to Evaluate X-ray Solution Scattering of Biological Macromolecules from Atomic Coordinates. *J. Appl. Crystallogr. 28*, 768−773.

(27) Krissinel, E., and Henrick, K. (2007) Inference of macromolecular assemblies from crystalline state. *J. Mol. Biol. 372*, 774−797.

(28) Mukherjee, A., Santra, M. K., Beuria, T. K., and Panda, D. (2005) A natural osmolyte trimethylamine N-oxide promotes assembly and bundling of the bacterial cell division protein, FtsZ and counteracts the denaturing effects of urea. *FEBS J. 272*, 2760−2772.

(29) Chebotareva, N. A., Andreeva, I. E., Makeeva, V. F., Livanova, N. B., and Kurganov, B. I. (2004) Effect of molecular crowding on self-association of phosphorylase kinase and its interaction with phosphorylase b and glycogen. *J. Mol. Recognit.: JMR 17*, 426−432.

(30) Webb, N. A., Mulichak, A. M., Lam, J. S., Rocchetta, H. L., and Garavito, R. M. (2004) Crystal structure of a tetrameric GDP-D-mannose 4,6-dehydratase from a bacterial GDP-D-rhamnose biosynthetic pathway. *Protein Sci. 13*, 529−539.

(31) Koropatkin, N. M., and Holden, H. M. (2005) Structure of CDP-D-glucose 4,6-dehydratase from Salmonella typhi complexed with CDP-D-xylose. *Acta Crystallogr. Sect. D, Biol. Crystallogr. 61*, 365−373.

(32) Minton, A. P. (2000) Implications of macromolecular crowding for protein assembly. *Curr. Opin. Struct. Biol. 10*, 34−39.

(33) Ellis, R. J. (2001) Macromolecular crowding: obvious but underappreciated. *Trends Biochem. Sci. 26*, 597−604.

(34) Nuss, J. E., Wanner, L. M., Tressler, L. E., and Bavari, S. (2010) The osmolyte trimethylamine N-oxide (TMAO) increases the proteolytic activity of botulinum neurotoxin light chains A, B, and E: implications for enhancing analytical assay sensitivity. *J. Biomol. Screening 15*, 928−936.

(35) Zhadin, N., and Callender, R. (2011) Effect of osmolytes on protein dynamics in the lactate dehydrogenase-catalyzed reaction. *Biochemistry 50*, 1582−1589.

(36) Hwang, H. Y., and Horvitz, H. R. (2002) The SQV-1 UDP-glucuronic acid decarboxylase and the SQV-7 nucleotide-sugar transporter may act in the Golgi apparatus to affect Caenorhabditis

elegans vulval morphogenesis and embryonic development. *Proc. Natl. Acad. Sci. U. S. A. 99*, 14218−14223.
(37) Schuck, P. (2003) On the analysis of protein self-association by sedimentation velocity analytical ultracentrifugation. *Anal. Biochem. 320*, 104−124.